Influence of closure on the 3D propagation of fatigue cracks in a nodular cast iron investigated by X-ray tomography and 3D Volume Correlation

Nathalie Limodin, Julien Réthoré, Jean-Yves Buffiere, François Hild, Stéphane Roux, Wolfgang Ludwig, Johann Rannou, Anthony Gravouil

Influence of closure on the 3D propagation of fatigue cracks in a nodular cast iron investigated by X-ray tomography and 3D Volume Correlation

Nathalie Limodin[a], Julien Réthoré[b], Jean-Yves Buffière[a], François Hild[c], Stéphane Roux[c], Wolfgang Ludwig[a,d], Johann Rannou[e] et Anthony Gravouil[b]

(a) Université de Lyon INSA-Lyon MATEIS CNRS UMR5510 Bat Saint Exupéry 20 Av. Albert Einstein, F-69621 Villeurbanne, France

(b) Laboratoire de Mécanique des Contacts et des Structures (LaMCoS), INSA-Lyon / UMR CNRS 5259, 20 avenue Albert Einstein, F-69621 Villeurbanne, France

(c) Laboratoire de Mécanique et Technologie (LMT-Cachan), ENS de Cachan / CNRS-UMR 8535, Université Paris 6, PRES UniverSud Paris, 61 Avenue du Président Wilson, F-94235 Cachan Cedex, France

(d) European Synchrotron Radiation Facility/Experimental Division (ESRF), BP 220, 6 rue J. Horowitz, F-38043 Grenoble, Cedex, France

(e) now at ONERA, DMSM, BP 72, 29 avenue de la Division Leclerc, F-92322 Châtillon, Cedex, France

Abstract

Synchrotron X-ray tomography was performed during in-situ fatigue crack propagation in two small size specimens made of nodular graphite cast iron. While direct image analysis allows to retrieve the successive positions of the crack front, and to detect local crack retardation, volume correlation enables for the measurement of displacement fields in the bulk of the specimen. The Stress Intensity Factors (SIF) which are extracted from the measured displacement fields and the corresponding local crack growth rate all along the front are in good agreement with published results. In particular, it is possible to link the non propagation

of a crack with crack closure in the COD maps or with a local value of the measured SIF range. It is shown that a non uniform closure process along the crack front induces an asymmetric arrest/growth of the crack.

Keywords: Synchrotron X-ray microtomography, 3D Digital Image Correlation, Crack propagation, Stress Intensity Factors, Nodular graphite cast iron

1. Introduction

Since the work of Paris and Erdogan [1] in the sixties, the most generally accepted formalism for describing the growth of fatigue cracks is the so called (empirical) Paris' law that relates the Fatigue Crack Growth Rate (FCGR) per cycle (da / dN) to the stress intensity factor range (ΔK). While many, more or less sophisticated, methods have been used to obtain experimental values of da / dN in cyclically loaded samples or components (see for example a review in [2] or [3]), the number of experimental methods giving access to ΔK has remained very limited, especially in optically opaque materials such as metals and alloys. This is because any experimental method aiming at "measuring" ΔK should in principle probe the strain field at the tip of the crack.

In the last ten years, however, important progress has been made in this field. Two different families of techniques have been used, namely, synchrotron X-ray diffraction and displacement field measurement either by Digital Image Correlation (DIC) or tracking of individual markers. Synchrotron X-ray diffraction studies allow mapping the crack tip strain field [4-7]. This method is mainly applied to unloaded samples and it focuses on measurement of the residual strains in the wake and at the tip of a post overload fatigue crack with a rather coarse spatial resolution along the crack front where the strain is averaged through the sample thickness for 1-mm thick samples where plane stress should prevail [7] or sampled every 300 µm to understand the stronger crack retardation observed near the specimen edges [5]. Such diffraction studies bring valuable insight into the overload

effect. For example, the post-overload residual strain was shown to persist after crack propagation with the overload response being "turned off" when loading above a critical load value [5]. However, no attempt was made to convert the measured strain maps into Stress Intensity Factors (SIFs) as has already been done in DIC studies. DIC has been used by various authors to map crack tip displacement fields at the specimen surface. Displacement fields are measured between a pair of images of the same specimen at different loads. It is then possible to extract the corresponding SIF of a crack [8-12]. For example, Hamam et al. [6] and Lopez-Crespo et al. [10] use DIC to evaluate the effect of crack tip plasticity on crack closure and to measure the corresponding effective SIF range. However, if 2D measurements of the SIF for crack opening, K_{op}, are relevant for thin specimens where plane stress condition prevails, they are not representative of the bulk behaviour of thick samples [13].

The development of X-ray tomography has now made it possible to visualize cracks in optically opaque materials like metals and alloys. In some cases, the tomography images can be used to evaluate 3D displacement fields near the crack tip in a specimen under load. Toda et al. [14; 15] used tracking of microstructural features, i.e. porosities, inside an Al alloy to map the 3D displacement field close to the crack tip in high resolution tomographic images, i.e. obtained with a synchrotron source. The markers are first identified by their centre of mass, and then they are individually tracked between 3D images of the same specimen under different loads in order to compute the global displacement field inside the specimen. This allows for the variation of SIF along the crack front to be extracted while direct image analysis allows for the Crack Opening Displacement (COD) to be retrieved [16]. Digital Volume Correlation (DVC) was also used to extract the COD maps in the cross-section of a pre-cracked specimen [17] while analysis of the measured 3D displacement field allowed for the SIFs to be computed [18]. It is to be emphasized that DVC, like the microstructural tracking method, can only be applied to materials with a suitable texture, i.e. materials that contain natural markers. Contrary to the 2D case, no "speckle pattern" can be

introduced in the specimen except by adding artificial markers at the material processing step [19] but then the risk to influence the material properties is high.

Some studies combine characterization of the crack-tip strain / displacement field with in-situ observation of crack propagation. Korsunsky et al. [6] use Synchrotron X-ray diffraction to gauge residual elastic strains through the thickness of unloaded samples. The comparison of the measured strain maps with Finite Elements Analysis was used to compute a residual stress intensity factor, K_{res}. An increased closure effect was observed after an overload. Then, the authors characterize crack opening during cyclic loading with 2D-DIC. Several studies combined marker tracking to obtain the 3D displacement field in the vicinity of the crack tip with tomography to visualize 3D cracks [16; 20] at different stages of crack propagation. Zhang et al. [16] studied 3D crack growth in an Al-Mg-Si alloy. Scans obtained at periodic intervals allowed them to follow crack shape, growth rate and opening in small size specimens ($0.6\times0.6\times12$ mm^3). Crack growth delay, which was observed in regions where crack segments overlap, could be correlated with Crack Tip Opening Displacement (CTOD) as a crack growth driving force. SIF measurements were also performed but larger values were unexpectedly correlated to smaller crack growth rate.

The material used in the present study was previously characterized using laboratory tomography during in-situ static tensile loading of a cracked specimen [18]. This analysis allowed for the quantification of crack closure through the determination of the opening stress intensity factor, K_{op}. The present investigation goes further by investigating the effect of closure on crack propagation. 3D displacement fields, COD maps, and SIFs have been obtained in-situ using DVC and synchrotron X-ray tomography at different stages of fatigue life. This complete 3D crack characterization in combination with image analysis and post-failure topography measurements allows for an interpretation of the crack propagation/arrest. It is shown that a non uniform closure level along the crack front induces asymmetric crack arrest/propagation of the crack.

2. Experimental methods

Material

The studied material is a nodular graphite cast iron (3.4 wt% C, 2.6 wt% Si, 0.05 wt% Mg, 0.19 wt% Mn, 0.005 wt% S, and 0.01 wt% P) with a fine dispersion of graphite nodules. Casting and appropriate heat treatments resulted in a ferritic matrix microstructure with a 14% volume fraction of graphite nodules with an average diameter of 45 μm. Young's modulus, yield stress and Poisson's ratio are equal to 175 GPa, 300 MPa, and 0.27, respectively. The difference in atomic numbers between carbon (nodules) and iron (matrix) results in a strong X-ray attenuation contrast so that the nodules, which are easily imaged by tomography, provide natural markers for volume correlation.

Pre-cracking in fatigue

To obtain small fatigue pre-cracked specimens, notched specimens with a 6×4 mm^2 cross-section were machined from the heat treated cast iron bar and loaded in fatigue at room temperature (load ratio = 0.1; frequency = 10 Hz). The specimen faces were mirror polished prior to fatigue experiment to allow for crack growth detection and monitoring with a travelling optical microscope. A load-shedding technique was used to maintain the maximum SIF (K_{max}) less than 12.8 MPa$\sqrt{\text{m}}$ so that confined plasticity prevails at the crack tip with a plastic zone size (in plane strain) smaller than 170 μm. Fatigue cycling was stopped when the observed crack was 1.5-mm long. For the tomography experiment, two smaller specimens with a 1.6×1.6 mm^2 cross-section were spark cut inside the large samples. One sample was cut from one side of a large pre-cracked specimen so that the crack tip experienced plane stress to plane strain conditions during fatigue pre-cracking. The other sample was cut in the mid-thickness of the large specimen where plane strain condition should prevail. For the sake of simplicity, the specimen cut at the former free surface (respectively former centre) of

the large pre-cracked sample is referred to as side specimen (respectively centre specimen) hereafter.

Synchrotron X-Ray tomography: In-situ propagation

The tomography experiment was performed on ID19 beamline at the European Synchrotron Radiation Facility (ESRF) in Grenoble, France. A monochromatic X-Ray beam ($\Delta\lambda/\lambda = 10^{-2}$) having a photon energy of 60 keV traverses the sample giving an incident-to-transmitted intensity ratio of about 10%. A Fast Readout Low Noise (FReLoN) 14-bit CCD camera with a 2048 $\times$ 2048 pixel chip was used. A specially designed fatigue machine allowing for in-situ loading and high frequency cycling (up to 50 Hz) of the specimens was used [21]. A PMMA tube, almost transparent to X-rays, was used as load rig. The machine was directly mounted on the rotating stage of the beam line. To obtain a complete scan of the specimen cross-section in the vicinity of the crack, six hundred radiographs were taken while the sample was rotating over 180 ° along its vertical axis; acquisition of a complete scan lasted about 42 minutes. Reconstruction of the tomographic data was performed with a standard filtered back-projection algorithm [22]. It provides a 3D image with a grayscale colourmap that is proportional to the local X-ray attenuation coefficient. Although better resolutions are achievable, a 5.06-µm voxel size was chosen as a compromise, namely, the image texture and the size of the reconstructed 3D images obtained from tomography. It is much smaller than the graphite nodule average size in order to allow for good quality images to be obtained while it is also large enough for the size of the region of interest, which was focused around the crack, to be only 340 $\times$ 340 $\times$ 512 voxels in size. This limited data size enabled for the DVC measurements to be performed on line during the tomography experiment (i.e., the computation time is less than the scan time on a PC with quad-core processor, and of the same order as the reconstruction duration).

In order to obtain 3D pictures of the specimen during the initial loading cycle, and thereafter for different stages of cyclic loading, the specimen was first gradually loaded up to a

maximum level, which is expected to result in a K_{max} value slightly less than that used for fatigue pre-cracking with a mean load that is adjusted to obtain a 0.1-load ratio during cycling under constant amplitude. At the beginning of the experiments, scans were acquired at intermediate loading steps from the maximum to the minimum load of the first unloading / loading cycle (Figure 1). Then during the in-situ fatigue experiment, scans were recorded at different time intervals with the specimen held under maximum load. When crack growth was detected in these images, e.g. after (n-1) cycles in Figure 1, another complete loading / unloading sequence was recorded. The fatigue experiment was conducted until the unbroken ligament became too short for further crack propagation.

Volume Correlation

3-D displacements of any voxel in the 3D volume are assessed by using a volume correlation technique. The principle of DVC is to analyze two images of the same specimen under different loading conditions, and to determine the displacement field in the bulk of the specimen by searching for the best match between the images. Recently, a new formulation has been proposed that allows one to decompose the displacement field onto an arbitrary chosen basis [23]. One such basis can be finite element shape functions in two or three dimensions. The latter will be used herein. In the present case, 3D reconstructed volumes are considered, and 8-node cubic elements defined on a 3D grid (tri-linear functions of x, y and z) may be chosen (it is designated as C8-DVC). The interested reader is referred to reference [23] for additional details on the DVC technique.

A Region Of Interest of $288 \times 288 \times 288$ voxels was centred in the original 3-D image. Elements with a 16-voxel edge were chosen as a good compromise between displacement uncertainty and spatial resolution of the displacement fields. For the selected size of elements, displacement uncertainty was assessed to be about 0.04 voxel. The reader is referred to [18] for details about the methodology of uncertainty evaluation.

For a given loading / unloading cycle, correlation was performed between the image obtained at the minimum load of the current cycle and the image obtained at the load for which the displacement field was sought. However, for the images that were obtained at different time intervals at the maximum load of a given cycle only, using the reference image of the previous loading cycle (see Figure 1) was thought to be accurate enough provided that the crack growth remained limited in the interval. In both specimens, correlation was performed from the 1st cycle until the stress in the un-cracked ligament had become too close to the yield stress for LEFM to be valid. Thus, analyses of the displacement field were restricted to 3,000 cycles for the centre specimen, and 49,000 cycles for the side specimen.

Due to the presence of the crack, the image obtained under higher load, i.e. the deformed image, cannot be perfectly matched to the reference image once it has been corrected for by the measured displacement field. The difference is the residual error that directly provides a 3D image of the crack [18]. Measurement of the SIF along the crack front was carried out using a method introduced by Hamam et al. [8] and adapted to 3D images [18]. The residual error is used to retrieve the crack position while the 3D displacement fields obtained with DIC are fitted in each plane orthogonal to the crack front with relevant mechanical equations in order to extract K_I, K_{II} and K_{III} SIF values along the crack front.

3. Results

Crack front location

Location of the crack front at different number of cycles can be obtained by direct image analysis of the 3D reconstructed data because the crack tip is visible under the maximum load of the fatigue cycle when the crack is open. Using ImageJ software [24], the voxel at the crack tip is manually selected in each slice ((y,z) plane containing the loading direction and perpendicular to the crack front, see Figure 2) and its coordinates are automatically recorded. This allows one to detect variations of the crack front position with increasing

number of cycles (Figure 2). The crack lengths measured at the specimen surface with an optical microscope, i.e. at a better resolution than the tomographic images, are also plotted for comparison purpose. The crack tip opening should fall within the resolution limits of the tomographic image (about twice the voxel size). However, the occurrence of phase contrast has probably allowed increasing the crack visibility in the absorption contrast images so that a good agreement is observed between the crack lengths measured either with tomography or with an optical microscope.

In the side specimen, the crack front is dissymmetric. It is 580-µm long close to the surface that corresponds to the former free surface of the large sample (named short crack side hereafter) and 796-µm long on the side that corresponds to the centre (called long crack side hereafter). In the centre specimen, the initial crack front is relatively straight with a crack length varying from 703 (short crack side) to 725 µm (long crack side).

The crack growth rate, da / dN, has been measured at each point along the crack front assuming a crack growth direction along the y axis for each and every point in Figure 2. The results are shown in Figure 3. In the side specimen, da / dN was uniform along the crack front so that the crack front shape remained invariant throughout propagation. However, the crack growth rate was almost zero before 32,500 cycles and became significant only after 40,000 cycles. With further propagation, da / dN increased uniformly along the crack front.

In the centre specimen, da / dN was initially not uniform along the crack front. After 2,000 cycles, the crack propagated at about 7×10^{-5} mm per cycle on the long crack side with a crack growth rate that decreased towards the short crack side where the crack was arrested. After 3,000 cycles, the crack started to propagate also on the short crack side so that after 3,500 cycles, a uniform value of 10^{-4} mm per cycle was reached all along the crack front.

COD maps and SIF extraction

The discontinuity in the u_z displacement field (induced by the presence of the crack) was used to measure the Crack Opening Displacements (COD) variation in the specimen cross-section. The displacement jump on the crack surface, or COD, was estimated from the difference between two slices taken parallel to the crack plane on either side of the crack discontinuity (see ref. [18] for details about COD measurement). The resulting COD maps are plotted in Figure 4 to Figure 7 for the side and centre specimen; the colourmap used is proportional to the value of crack opening in voxels. From the a priori uncertainty analysis, it was concluded that a 0.12-voxel COD, i.e. three times the measurement standard uncertainty, corresponds to a real opening and that COD levels less than that value could not be distinguished from local crack closure [18]. The limit for crack opening, i.e. 0.12 voxel, was plotted as a white line on the COD maps. Detailed analysis of loading / unloading cycle at different numbers of fatigue cycles was performed to detect crack opening / closure.

From the 3-D displacement field, SIF values could be extracted along the crack front by analysing this displacement field in terms of selected mechanically relevant fields [16]. Then, the comparative analysis of the COD maps with SIF values along the crack front in Figure 4 to Figure 7 allows for the detection of local crack closure / opening and the determination of the corresponding SIF values. The SIF range for crack opening, ΔK_{op}, reported in ref. [18] was plotted as a dashed line for comparison purposes.

In the side specimen, the COD at the tip appears very uniform along the crack front during all the fatigue life. In the first cycle (Figure 4), at 86N, the crack was closed at its tip and opened upon loading at 153N ($\Delta K_I \approx 7$ MPa$\sqrt{\text{m}}$) although areas of local closure still existed on the long crack side ($\Delta K_I \approx 6.5$ MPa$\sqrt{\text{m}}$), see arrow in Figure 4. The ΔK_I values shown in Figure 4 were obtained for loads varying between 14 N and 228 N. The fatigue cycles were performed between $F_{max} = 190$ N and $F_{min} = 19$ N. Based on Figure 4 one can therefore assume that during cycling ΔK_I ranged between 8 and 11 MPa$\sqrt{\text{m}}$. Upon unloading down to 114 N, the

crack closed rather uniformly at the tip for ΔK_I less than 6.5 MPa√m. Although the crack was not observed to grow (Figure 2), the CTOD increased progressively from less than 0.3 to a uniform value of 0.4 voxel. After 45,000 fatigue cycles (Figure 5), unloading from 186 N to 99 N allowed the crack to close uniformly at its tip as ΔK_I decreased from 11.5 to 6.5 MPa√m. At 77 N, the crack was firmly closed ($\Delta K_I \approx 4$ MPa√m). After 49,000 cycles, the crack has grown by about 100 µm farther and the COD maps, not presented here, show that the crack closed upon unloading at 49 N, i.e. for ΔK_I around 6.5 MPa√m, while it was still open at 92 N.

In the centre specimen, the COD map was not symmetric with respect to the crack front (Figure 6). At the first loading cycle, the crack has opened upon loading at 234 N and ΔK_I has reached a higher value on the long crack side ($\Delta K_I \approx 15$ MPa√m) than on the short crack side ($\Delta K_I \approx 9$ MPa√m). Upon unloading, the short crack side closed first at 164 N ($\Delta K_I \approx 7$ MPa√m) and almost complete closure was obtained along the crack front at 94 N ($\Delta K_I \approx 6.5$ MPa√m) with only local opening on the long crack side. After 3,000 cycles (Figure 7), the crack has opened on both sides under maximum load and it stayed open even when unloading down to 92N ($\Delta K_I \geq 6.5$ MPa√m). The dissymmetry in crack opening that was observed in the 1st cycle between both sides of the specimen persisted so that the COD remained smaller on the short crack side.

4. Discussion

The comparison of COD maps with local SIF values along the crack front shows that the SIF range for crack opening, ΔK_{op}, is about 6.5 MPa√m for the two specimens of this study. This value is consistent with previous measurements performed by the authors for the same material using a laboratory x-ray source [18]. When the crack propagates, the load for crack opening / closure was observed to decrease slightly resulting in a constant value of ΔK_{op}. The same trend was reported by Nadot [25] although with a smaller ΔK_{op} value. For both specimens, large values of crack opening were correlated with large values of SIF. However,

it appears that the crack being opened is a necessary but not sufficient condition for crack propagation. In both specimens, the COD maps show that the crack was open under the maximum load of the fatigue cycle. The difference in crack propagation behaviour between the side and centre specimens when submitted to similar fatigue loading conditions therefore requires a more detailed analysis.

From the crack growth rates reported in Figure 3 and the ΔK_I values reported in Figure 4b to Figure 7b, it is possible to plot a da / dN-ΔK_I curve (Figure 8). For comparison purposes, the crack growth law obtained by Dierickx [26] for long cracks in large CT specimens from the same material and the crack growth threshold obtained by Nadot [27] for a similar cast iron are also plotted.

In the side specimen, the crack was initially not uniform in length due to crack tunnelling effect. In the larger sample, a stronger closure effect at the specimen surface than at mid-thickness has resulted in a smaller crack length at the free surface [3], i.e. the short crack side in the side specimen (Figure 2a). However, the difference in crack length between both sides of the side specimen was 200 µm only so that the computed ΔK_I value increased almost negligibly from the short to the long crack sides and, at the first cycle, ΔK_I showed a rather uniform value of about 10 MPa$\sqrt{m}$ along the crack front. This value was proved insufficient to re-start the crack propagation even after 32,500 cycles as shown in Figure 2a. Thus, in Figure 8a, at 32,500 and 40,000 cycles, the average value of ΔK_I for the maximum load of the 1st cycle was used as an estimate for the value of ΔK_I in the following fatigue cycles in the absence of significant crack growth. A ΔK_I range close to 10 MPa$\sqrt{m}$ therefore resulted in a crack growth rate smaller than 10^{-5} mm per cycle. Although cutting of the small tomography sample may have induced stress relaxation as compared to the stress state that formerly existed inside the larger specimen, we can assume that the crack was initially closed during a large fraction of the fatigue cycle due to the influence of the large plane stress plastic zone size inherited from the larger specimen precracking. This plane stress

plastic zone is known to enhance closure near the free surface with a zone of influence that may extend deeply inside thin specimens [28].Thus, until 40,000 cycles, the COD / ΔK_I maximum value increased without noticeable crack growth as the crack has to overcome the effect of Plasticity Induced Crack Closure. Then at 45,000 cycles and later, ΔK_I values largely above 10 MPa√m, i.e. larger than ΔK_{op}, arose and the corresponding crack growth rates increased concomitantly in agreement with Dierickx' [26] data. From these results, the threshold value for crack growth is estimated to be about 10 MPa√m. No detailed measurement of ΔK_{th} has been performed by Dierickx, but Nadot reported a similar value of 8.6 MPa√m for a similar, although not identical, nodular graphite cast iron.

In the centre specimen, the crack has initially a fairly constant length throughout the sample thickness (Figure 2b). However in spite of this limited variation in crack length, the measured SIF value increased in a markedly different way from the "short" ("S" in Figure 8b) to the "long" ("L" in Figure 8b) crack side (10 to 15 MPa√m respectively). At the first cycles, this large variation in ΔK_I along the crack front resulted in a large variation in crack growth rates with a crack that grew rapidly on the long crack side, while it was pinned on the short crack side where the ΔK_I value is locally below the crack growth threshold estimated for the side specimen. As shown in Figure 8b, the crack propagation required 3,000 cycles to start on the short crack side, when ΔK_I reached a value of about 12 MPa√m, i.e. close to the value used for fatigue pre-cracking. Then, the difference in crack growth rates between both sides of the specimen progressively reduced. However, the reasons for the COD / ΔK_I values being initially larger on the long than on the short crack side are not straightforward. In the present case, Plasticity Induced Crack Closure is unable to explain the decrease in COD / ΔK_I on the short crack side as the sample was cut from the mid-thickness of the large sample where plane strain conditions should prevail and where a uniform plastic zone size is expected.

Analysis of crack topography was thus performed to assess the possible influence of the roughness of the crack surfaces inherited from the larger specimens on subsequent crack

propagation. After the fatigue tests, the specimens were broken in bending to allow for their analysis in a laser profilometer. The results are shown in Figure 9 where similar roughness scales were used to allow for a direct comparison of the two specimens. Crack tip positions from Figure 2 were superimposed on the roughness maps to visualize the possible correlation between crack growth and roughness. The crack topography in the side specimen is rather smooth in the crack tip area, especially at the position of the initial crack front ('0k' in Figure 9a).

In the centre specimen however, a significant step of 85-µm in height, i.e. larger than the average size of the graphite nodules, is observed on the left hand side of the topography map near the short crack side. This step was inherited from the larger pre-cracked sample and the reasons for its occurrence could not be guessed from the observation of microstructure inside the small tomography sample. However, it is clear that this asperity affected the propagation of the crack as there is a strong correlation between the crack front region where the crack was arrested for almost 3,000 cycles (see '0k' vs. '3k' in Figure 9b) and this bifurcation in the crack path. Reasons for crack delay in the centre specimen may now be understood from the comparison of the topography with the COD maps or with crack growth rates. As shown in Figure 10, the depth extent of the step in the crack plane correlates both with a local decrease in COD and with a drop in the da / dN value along the crack front. It is expected that the presence of the step in the crack plane induce mode II/mode III displacements with corresponding non-zero K_{II}/K_{III} values that have a shielding effect on Mode I opening [29]. Figure 11 shows the variations of ΔK_{II} and ΔK_{III} with sample thickness after 3000 cycles. The values of ΔK_{II} mainly fluctuate around zero but a small "peak" may be guessed at the step location. ΔK_{III} has a more constant value of -0.5 MPa$\sqrt{m}$ that increases slightly in absolute value towards the step. To better capture the SIF mode mixity in this region, and validate our interpretation, a denser displacement mapping would be needed.

5. Conclusions

3D propagation of a fatigue crack in a cast iron sample has been characterized in situ by synchrotron x-ray microtomography and DVC. Tomography images provide local crack growth rates while DVC is used to extract COD maps and local SIF values.

A crack with mixed plane stress to plane strain condition along its front (“side specimen”) remains arrested for more than 40,000 cycles. This retardation is attributed to PICC that may extend deep below the surface of the large pre-cracked sample. When submitted to similar conditions of loading, a crack under initial plane strain condition (“centre specimen”), i.e. without the influence of plane stress PICC, propagates along most of the front as soon as the cyclic loading starts but remains pinned locally near an edge. A Post-mortem analysis of the crack surface topography shows this pinning correlates with a salient asperity producing a step along the crack front. The analysis of the two specimens of the present study shows that the 6.5-MPa$\sqrt{m}$ value for crack opening is of the same order as that obtained from in-situ tensile loading with a lab CT [18].

The combination of 3D image analysis to visualize the crack, COD analysis made accessible thanks to measured displacements, and SIF computation (extracted from the measured displacements) along the crack front is the first step towards a more complete understanding of 3D crack growth.

However, in-situ tensile loading of “centre” and “side” specimens is planned in order to clarify a possible difference in opening behaviour at a finer image resolution.

6. Acknowledgments

This work was funded by the CETIM Foundation grant entitled PROPAVANFIS: ‘Advanced methods for the experimental and numerical analyses of crack propagations under complex

loadings.' This work was also made possible by an ESRF grant for the experiment MA-501 on ID19 beamline.

7. References

[1] Paris PC, Erdogan FA: A Critical Analysis of Crack Propagation Laws. *Journal of Basic Engineering, Transactions, ASME, Series D* 1963, 85:528-534.

[2] Hudak S, Bucci R: Fatigue Crack Growth Measurement and Data Analysis. *ASTM STP738* 1981:367.

[3] Schijve J: *Fatigue of structures and materials*. Kluwer Academic; 2001.

[4] Croft M, Zhong Z, Jisrawi N, Zakharchenko I, Holtz R, Skaritka J, Fast T, Sadananda K, Lakshmipathy M, Tsakalakos T: Strain profiling of fatigue crack overload effects using energy dispersive X-ray diffraction. *International Journal of Fatigue* 2005, 27:1408-1419.

[5] Croft M, Shukla V, Jisrawi N, Zhong Z, Sadangi R, Holtz R, Pao P, Horvath K, Sadananda K, Ignatov A, Skaritka J, Tsakalakos T: Mapping and load response of overload strain fields: Synchrotron X-ray measurements. *International Journal of Fatigue* 2009, 31:1669-1677.

[6] Korsunsky AM, Song X, Belnoue J, Jun T, Hofmann F, De Matos PF, Nowell D, Dini D, Aparicio-Blanco O, Walsh MJ: Crack tip deformation fields and fatigue crack growth rates in Ti-6Al-4V. *International Journal of Fatigue* 2009, 31:1771-1779.

[7] Steuwer A, Edwards L, Pratihar S, Ganguly S, Peel M, Fitzpatrick ME, Marrow TJ, Withers PJ, Sinclair I, Singh KD, Gao N, Buslaps T, Buffiere JY: In situ analysis of cracks in structural materials using synchrotron X-ray tomography and diffraction. *Nuclear Instruments and Methods in Physics Research, Section B: Beam Interactions with Materials and Atoms* 2006, 246:217-225.

[8] Hamam R, Hild F, Roux S: Stress intensity factor gauging by digital image correlation: Application in cyclic fatigue. *Strain* 2007, 43:181-192.

[9] McNeill SR, Peters WH, Sutton MA: Estimation of stress intensity factor by digital image correlation. *Engineering Fracture Mechanics* 1987, 28:101-112.

[10] Lopez-Crespo P, Shterenlikht A, Yates JR, Patterson EA, Withers PJ: Some experimental observations on crack closure and crack-tip plasticity. *Fatigue & Fracture of Engineering Materials & Structures* 2009, 32:418-429.

[11] Roux S, Hild F: Stress intensity factor measurements from digital image correlation: Post-processing and integrated approaches. *International Journal of Fracture* 2006, 140:141-157.

[12] Yoneyama S, Ogawa T, Kobayashi Y: Evaluating mixed-mode stress intensity factors from full-field displacement fields obtained by optical methods. *Engineering Fracture Mechanics* 2007, 74:1399-1412.

[13] de Matos P, Nowell D: Experimental and numerical investigation of thickness effects in plasticity-induced fatigue crack closure. *International Journal of Fatigue* 2009, 31:1795-1804.

[14] Toda H, Sinclair I, Buffiere JY, Maire E, Connolley T, Joyce M, Khor KH, Gregson P: Assessment of the fatigue crack closure phenomenon in damage-tolerant aluminium alloy by in-situ high-resolution synchrotron X-ray microtomography. *Philosophical Magazine* 2003, 83:2429-2448.

[15] Toda H, Sinclair I, Buffiere JY, Maire E, Khor KH, Gregson P, Kobayashi T: A 3D measurement procedure for internal local crack driving forces via synchrotron X-ray microtomography. *Acta Materialia* 2004, 52:1305-1317.

[16] Zhang H, Toda H, Qu P, Sakaguchi Y, Kobayashi M, Uesugi K, Suzuki Y: Three-dimensional fatigue crack growth behavior in an aluminum alloy investigated with in situ high-resolution synchrotron X-ray microtomography. *Acta Materialia* 2009, 57:3287-3300.

[17] Réthoré J, Tinnes J, Roux S, Buffière J, Hild F: Extended three-dimensional digital image correlation (X3D-DIC). *Comptes Rendus Mécanique* 2008, 336:643-649.

[18] Limodin N, Rethore J, Buffiere J, Gravouil A, Hild F, Roux S: Crack closure and stress intensity factor measurements in nodular graphite cast iron using three-dimensional correlation of laboratory X-ray microtomography images. *Acta Materialia* 2009, 57:4090-4101.

[19] Nielsen SF, Poulsen HF, Beckmann F, Thorning C, Wert JA: Measurements of plastic displacement gradient components in three dimensions using marker particles and synchrotron X-ray absorption microtomography. *Acta Materialia* 2003, 51:2407-2415.

[20] Qu P, Toda H, Zhang H, Sakaguchi Y, Qian L, Kobayashi M, Uesugi K: Local crack driving force analysis of a fatigue crack by a microstructural tracking method. *Scripta Materialia* 2009, 61:489-492.

[21] Buffiere JY, Ferrie E, Proudhon H, Ludwig W: Three-dimensional visualisation of fatigue cracks in metals using high resolution synchrotron X-ray micro-tomography. *Materials Science and Technology* 2006, 22:1019-1024.

[22] Kak AC, Slaney M: *Principles of Computerized Tomographic Imaging*. Society of Industrial and Applied Mathematics; 2001.

[23] Roux S, Hild F, Viot P, Bernard D: Three-dimensional image correlation from X-ray computed tomography of solid foam. *Composites Part A: Applied Science and Manufacturing* 2008, 39:1253-1265.

[24] [http://rsb.info.nih.gov/ij/]

[25] Nadot Y: Influence des défauts de fonderie sur la résistance à la fatigue d'une fonte GS (in french). *PhD thesis.* Ecole Nationale Supérieure de Mécanique et d'Aérotechnique et Faculté des Sciences Fondamentales et Appliquées, 1997.

[26] Dierickx P: Etude de la microstructure et des mecanismes d'endommagement de fontes G.S. ductiles : influence des traitements thermiques de ferritisation (in french). *PhD thesis.* INSA de Lyon, 1996.

[27] Nadot Y, Ranganathan N, Mendez J, Beranger AS: Study of natural cracks initiated on casting defects by crack front marking. *Scripta Materialia* 1997, 37:549-553.

[28] Chermahini R, Shivakumar K, Newman Jr J, Blom A: Three-Dimensional aspects of plasticity-induced fatigue crack closure. *Engineering Fracture Mechanics* 1989, 34:393-401.

[29] Suresh S: *Fatigue of Materials*. Cambridge University Press; 1998.

8. Figure captions

Figure 1: In-situ propagation experiments. The reference image used for DIC at cycles $1 \leq N \leq n - 1$ is the image at F_{min} of the first cycle.

Figure 2: Change of the crack front location with the number of fatigue cycles in (a) the side and (b) the centre specimen as determined from the reconstructed 3D images. Crack growth is along the *y* axis and loading along *z*.

Figure 3: Crack growth rate change along the crack front with the number of cycles in the (a) side and (b) centre specimens.

Figure 4: (a) COD maps for different load levels. The crack front position at F_{max} in Figure 2a is depicted with dots and the boundary of the open crack region is plotted as a white line. (b) ΔK_I values along the crack front in the side specimen during loading for the 1st cycle. The ΔK_{op} value reported in ref. [18] is represented with a dashed line in Figure 4b to Figure 7b.

Figure 5: (a) COD maps for different load levels. (b) ΔK_I values along the crack front in the side specimen during unloading after 45,000 cycles

Figure 6: (a) COD maps for different load levels. (b) ΔK_I values along the crack front in the centre specimen during unloading at the first cycle

Figure 7: (a) COD maps for different load levels. (b) ΔK_I values along the crack front in the centre specimen during unloading at 3,000 cycles

Figure 8: da / dN - ΔK_I curves: experimental points in the (a) side and (b) centre specimen and literature data. For the centre specimen, the local values corresponding to the short crack side and long crack side are identified by letters (“S” and “L”) and are attributed the colour of their corresponding cycle. The vertical dashed line shows the ΔK_{th} value determined by Nadot [25].

Figure 9: Topography of the crack surface in the (a) side and (b) centre specimen. The location of the crack front at different fatigue cycles is superimposed.

Figure 10: Comparison of crack topography (same scale as in Figure 9) with COD map (same scale as in Figure 6) and crack growth rates. (Note that for comparison purposes the maps have been rotated as compared to Figs. 6 and 9)

Figure 11: Variation of SIF range in modes II and III with position along the crack front. The step extent in the crack surface is indicated with a dashed line.

Figure(s)

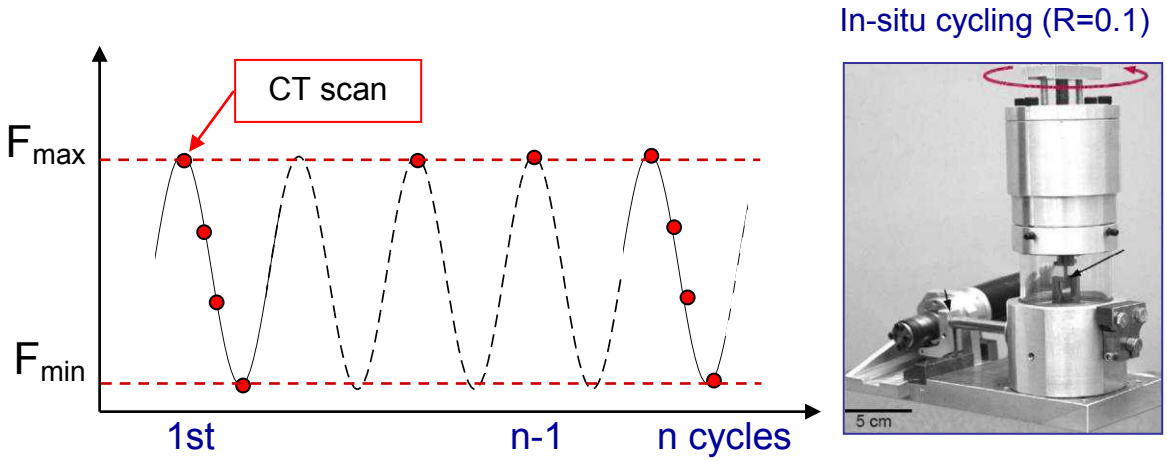

Figure 1: In-situ propagation experiments. The reference image used for DIC at cycles $1 \leq N \leq n-1$ is the image at F_{min} of the first cycle.

Figure(s)

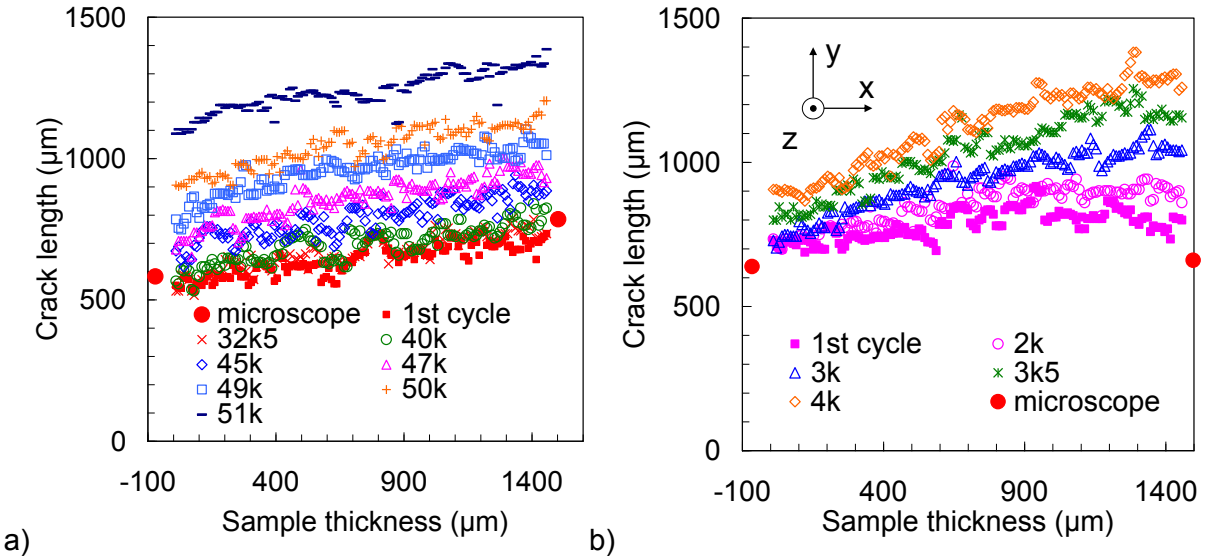

Figure 2: Change of the crack front location with the number of fatigue cycles in (a) the side and (b) the centre specimen as determined from the reconstructed 3D images. Crack growth is along the *y* axis and loading along *z*.

Figure(s)

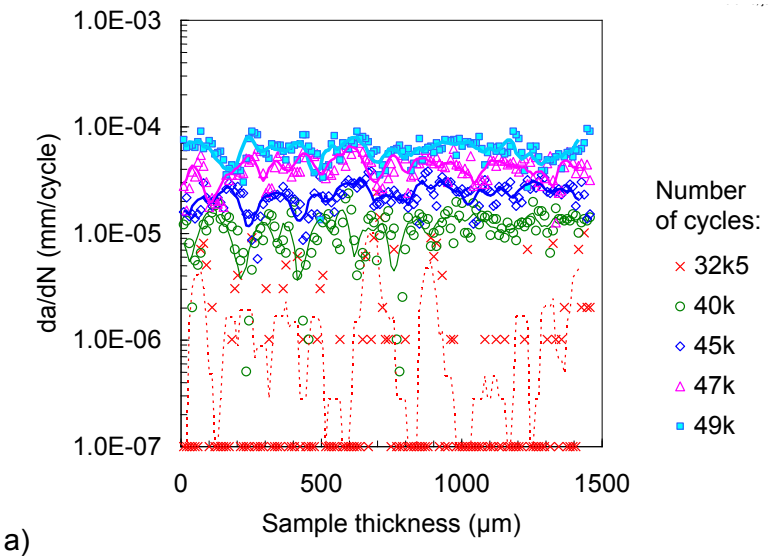

a)

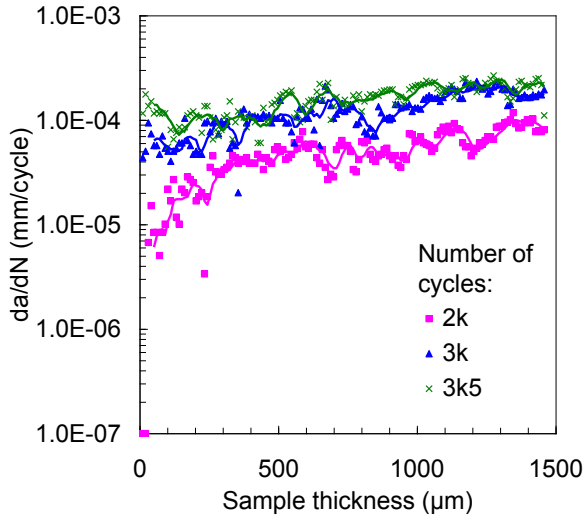

b)

Figure 3: Crack growth rate change along the crack front with the number of cycles in the (a) side and (b) centre specimens.

Figure(s)

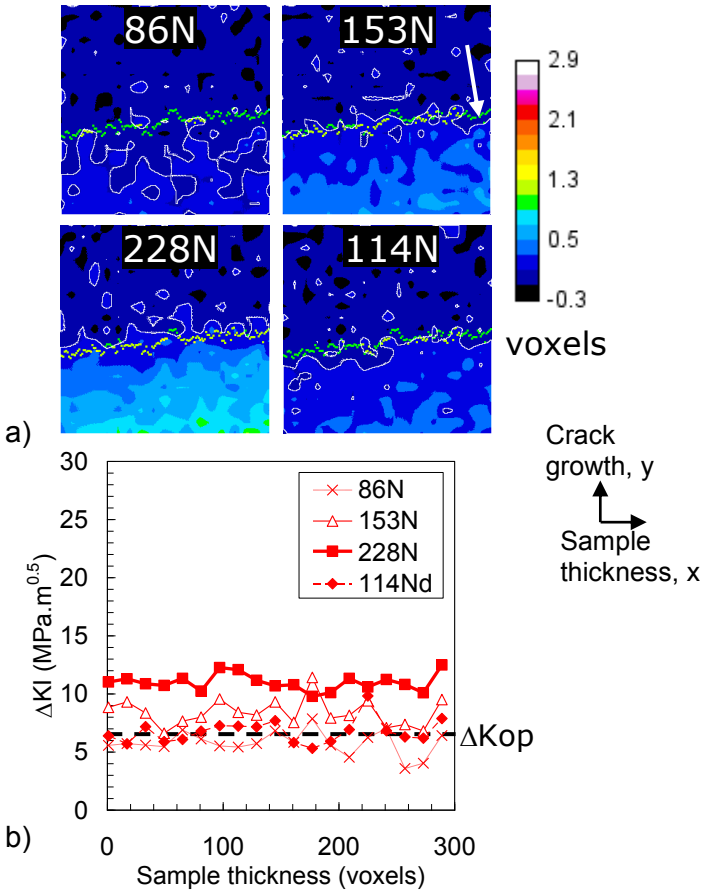

Figure 4: (a) COD maps for different load levels. The crack front position at F_{max} in Figure 2a is depicted with dots and the boundary of the open crack region is plotted as a white line. (b) ΔK_I values along the crack front in the side specimen during loading for the 1st cycle. The ΔK_{op} value reported in ref. [18] is represented with a dashed line in Figure 4b to Figure 7b.

Figure(s)

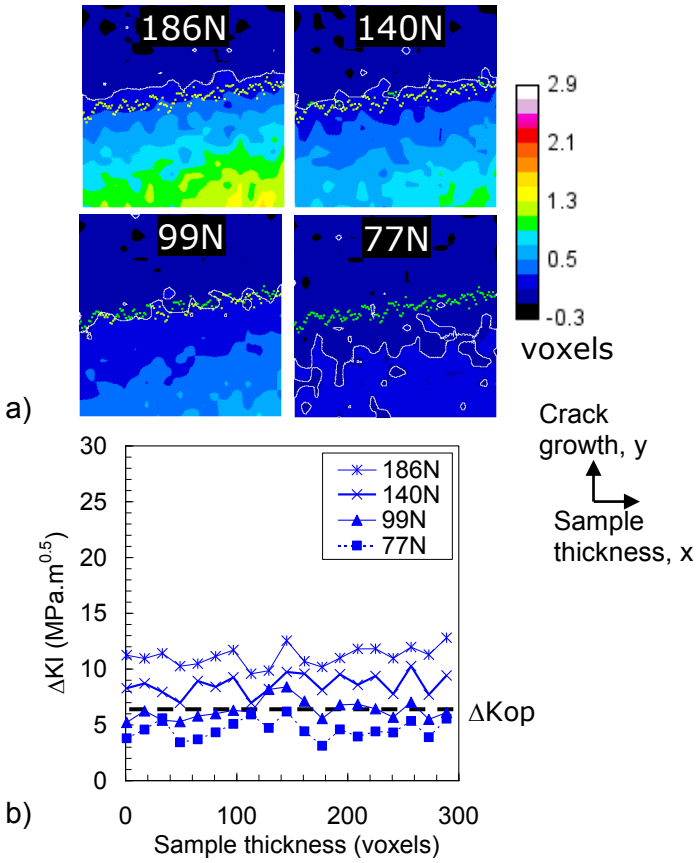

Figure 5: (a) COD maps for different load levels. (b) ΔK_I values along the crack front in the side specimen during unloading after 45,000 cycles

Figure(s)

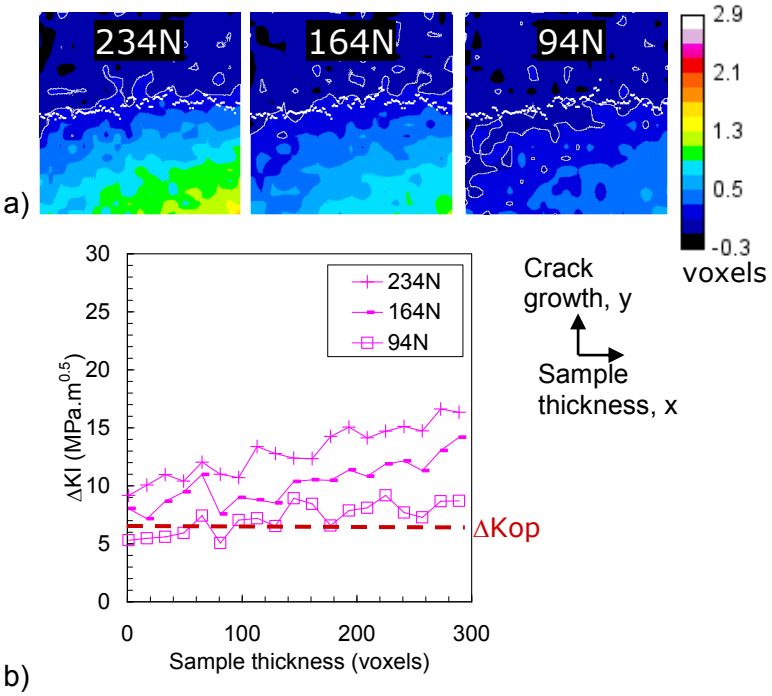

Figure 6: (a) COD maps for different load levels. (b) ΔK_I values along the crack front in the centre specimen during unloading at the first cycle

Figure(s)

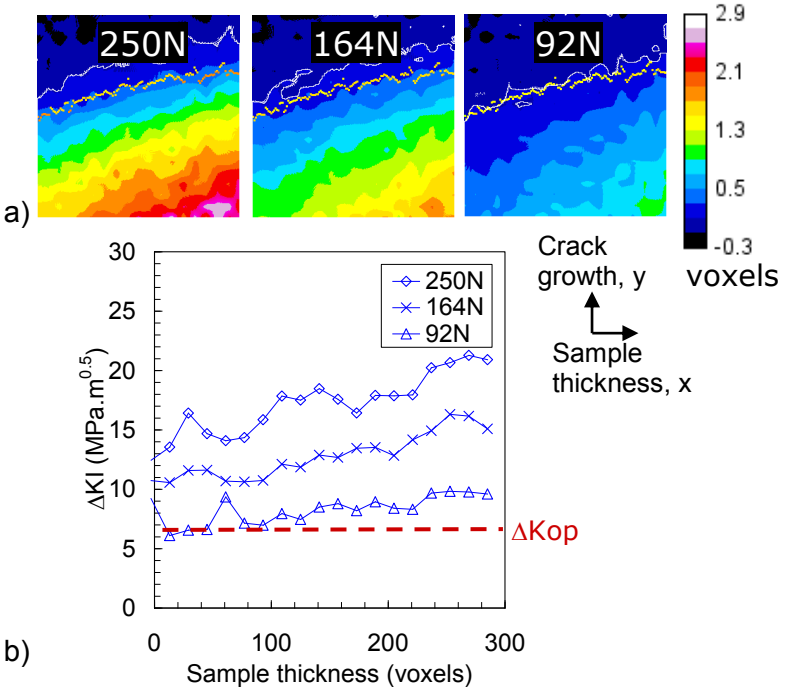

Figure 7: (a) COD maps for different load levels. (b) ΔK_I values along the crack front in the centre specimen during unloading at 3,000 cycles

Figure(s)

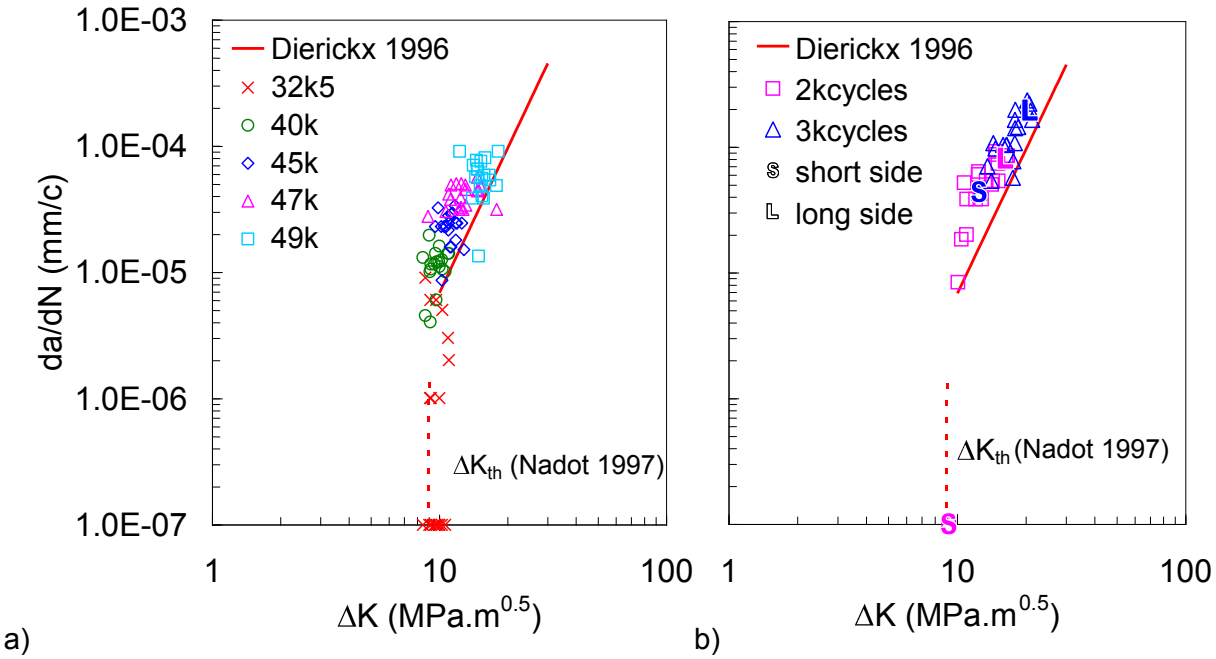

Figure 8: d*a* / d*N* - ΔK_I curves: experimental points in the (a) side and (b) centre specimen and literature data. For the centre specimen, the local values corresponding to the short crack side and long crack side are identified by letters ("S" and "L") and are attributed the colour of their corresponding cycle. The vertical dashed line shows the ΔK_{th} value determined by Nadot [25].

Figure(s)

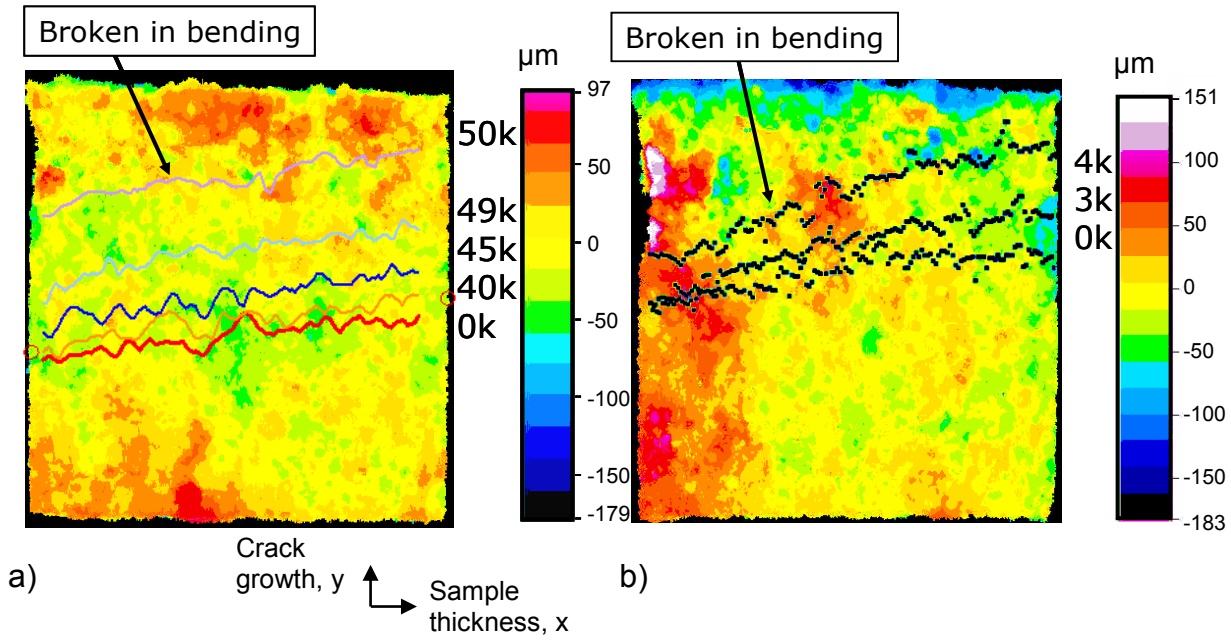

Figure 9: Topography of the crack surface in the (a) side and (b) centre specimen. The location of the crack front at different fatigue cycles is superimposed.

Figure(s)

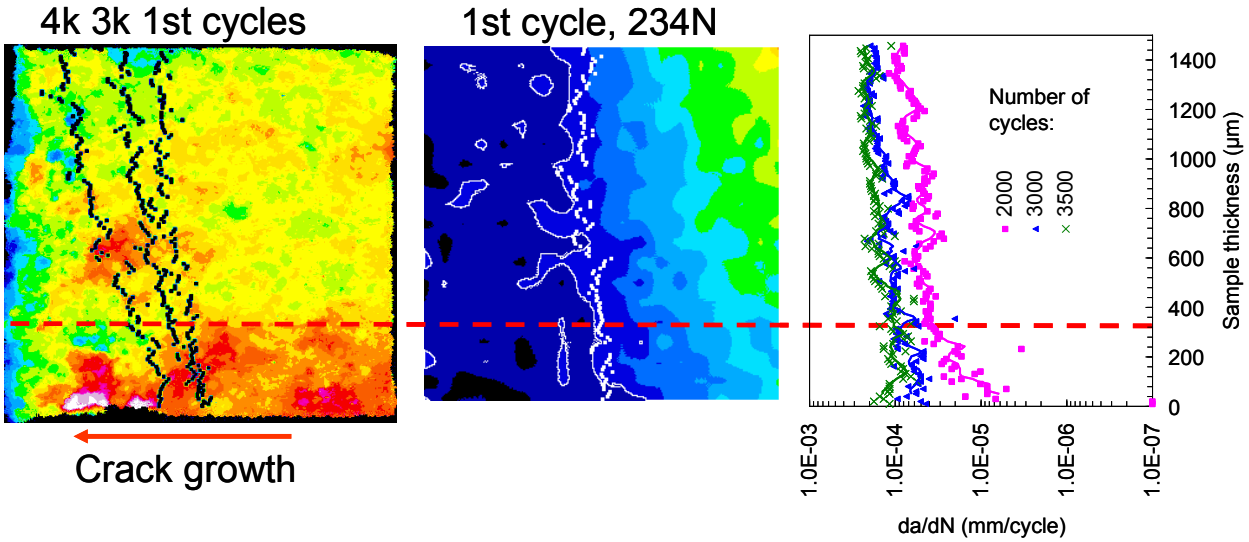

Figure 10: Comparison of crack topography (same scale as in Figure 9) with COD map (same scale as in Figure 6) and crack growth rates. (Note that for comparison purposes the maps have been rotated as compared to Figs. 6 and 9)

Figure(s)

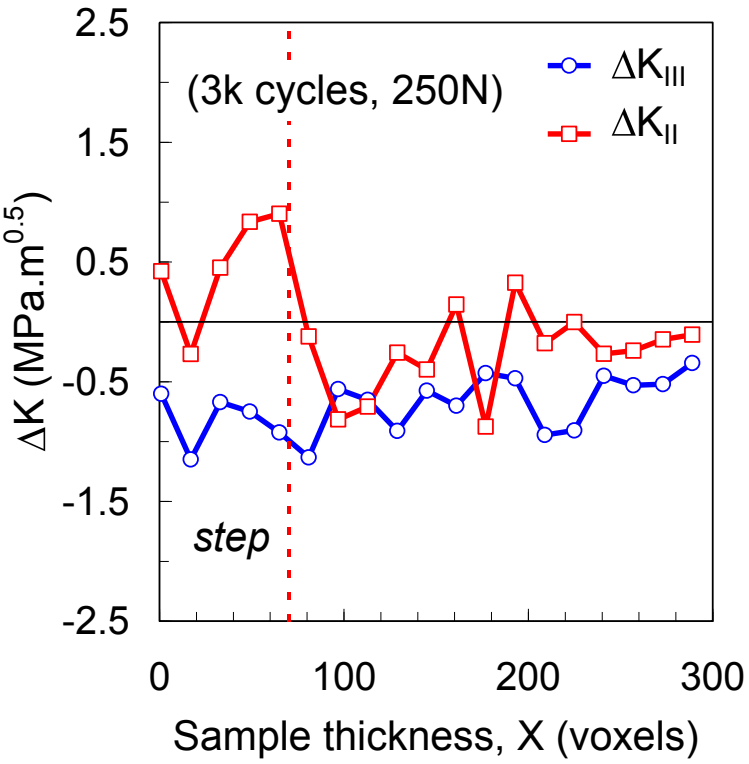

Figure 11: Variation of SIF range in modes II and III with position along the crack front.

The step extent in the crack surface is indicated with a dashed line.